ChemComm

Accepted Manuscript

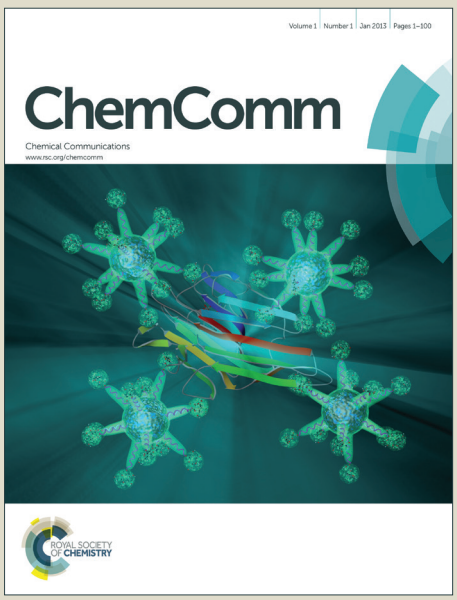

ROYAL SOCIETY OF CHEMISTRY

www.rsc.org/chemcomm

Chemical Communications ChemComm

Cite this: DOI: 10.1039/c0xx00000x

www.rsc.org/xxxxxx

COMMUNICATION

NiSb Alloy Hollow Nanospheres as Anode Materials for Rechargeable Lithium Ion Batteries

Hongshuai Hou, Yingchang Yang, Laibing Fang, Chengchi Pan, Xuming Yang, Weixin Song, Xiaobo Ji*

Received (in XXX, XXX) Xth XXXXXXXXX 20XX, Accepted Xth XXXXXXXXX 20XX

DOI: 10.1039/b000000x

NiSb alloy hollow nanospheres (HNSs) obtained by galvanic replacement were firstly applied as anode materials for lithium ion batteries, giving the best electrochemical performances for NiSb alloy materials so far with high reversible capacity of 420 mAh g^{-1} after 50 cycles, close to its theoretical capacity (446 mAh g^{-1}).

Hollow micro/nanostructures with well-defined morphology, high surface area, low density, high loading capacity and shell permeability have attracted considerable attention as an important branch of advanced functional materials. The unique feature of hollow micro/nanostructures has rendered them greatly promising application in energy storage and conversion, catalysis, drug delivery, gas sensing and biomedicine.[1,2]

Galvanic replacement reaction has been demonstrated as an efficient way to fabricate hollow nanostructures including nanoboxes,[3] nanospheres,[4,5] nanotubes.[6,7] For this galvanic replacement to take place, metal ions must have higher redox potential than that of the template material. In principle, this particular reaction should occur between any two metals with the favorable reduction potentials difference. [8] In fact, the results could be completely different from what one would expect due to the effect of reaction kinetics. Up to now, only few metals have been reported as successful template materials for the galvanic replacement.

Sb has attracted considerable attention in lithium ion batteries, because of its high Li storage capacities, flat potential curve (due to the presence of only a single intermediate phase in its reaction with lithium) and more positive Li intercalation voltages than that of graphite, which minimizes the risk of Li dendrite formation during fast recharge. However, the lithiation process in Sb results in significant volume expansion (up to 150%), leading to poor cycle performance. It is suggested that Sb alloys including NiSb, $CoSb_3$, ZnSb, Cu_2Sb and SnSb have been proposed to reduce the drastic volume changes and thus to extend the cycle life of this material. [9-12]

In this paper, we firstly reported the preparation of NiSb alloy HNSs by undertaking galvanic replacement. The unique bimetallic hollow structure can alleviate the volume change, resulting in the reduction of transport lengths for both mass and charge transport. Thus, the NiSb alloy HNSs electrode exhibited excellent cycle stability and rate performance in lithium ion batteries. It is believed that this green and convenient method will broaden new routes toward synthesizing other advanced energy-storing materials.

Fig. 1a and b showed the Scanning Electron Microscope (SEM) images of original Ni templates with rough surfaces and the diameters were in the range of 50-80 nm. Fig. 1c and d showed the SEM images of NiSb alloy HNSs obtained via galvanic replacement. From low magnification SEM image of the as-prepared NiSb alloy HNSs in Fig. 1c, it is shown that the as-prepared products displayed spherical morphology, with a uniform size distribution ranging from 70 to 100 mm. The NiSb alloy hollow nanostructure inherited the spherical morphology of original Ni nanosphere template. The interior structures of the prepared NiSb alloy HNSs can be revealed by the SEM images of broken spheres and the wall thickness was about 15 nm. Fig. 1d gave magnified SEM images of the spherical NiSb samples collapsed or broken, clearly showing hollow characteristic structure for the synthesized spherical NiSb samples.

Fig. 2a showed the Transmission Electron Microscope (TEM) image of original Ni templates with spherical morphology and solid interior in accord with the SEM results. The hollow interior and detailed geometrical structure of the as-prepared NiSb alloy NSs were directly elucidated by TEM observation in Fig.2 b, c. In good agreement with the SEM results, hollow structures can be observed and the inner cavities are clearly revealed by the sharp contrast between the NiSb shells and hollow interiors. The high resolution TEM (HRTEM) image (Fig. 2d) and selected area electron diffraction (SAED) (Fig. 2d inset) clearly showed the polycrystalline texture of the NiSb alloy HNSs.

The X-ray Diffraction (XRD) results were shown in Fig. 3. The original Ni nanosphere template was identified on the basis of the clearly distinguishable diffraction peaks at 44.493°, 51.846° and 76.376°, corresponding to (1 1 1), (2 0 0) and (2 2 0) crystal planes of Ni. The peaks around 31.479°, 34.910°, 44.121°, 56.888°, 59.102°, 60.466°, 65.712°, 73.726°, 76.129° and 79.258° were observed, corresponding to (1 0 1), (0 0 2), (1 0 2), (1 1 0), (2 0 1), (1 1 2), (1 0 3), (2 0 2), (0 0 4), (2 1 1) and (2 0 3) crystal planes of NiSb alloy, no secondary phases were observable, the as-prepared NiSb alloy HNSs with polycrystalline texture were identified, which was in good agreement with HRTEM and SAED results (Fig. 2d).

Scheme 1 illustrated the proposed mechanism for the growth of NiSb HNSs. Since the Ni is more active than Sb, Ni atom was oxidized to Ni^{2+} and Sb^{3+} was simultaneously reduced to Sb atom when it contacted with Sb^{3+} in solution (step 1). Meanwhile, the newly generated Sb atoms after the galvanic replacement were

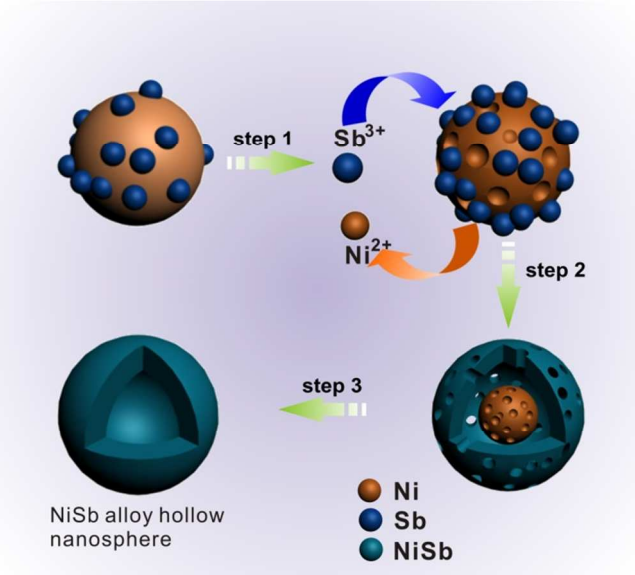

Scheme 1 A schematic of NiSb alloy hollow nanosphere formation during the galvanic replacement at different stages.

coated on the surface of Ni nanosphere template and formed NiSb alloy with Ni. Since the replacement reaction was initiated locally rather than over the entire surface, the coating would lead to the formation of a porous NiSb shell on each individual Ni nanosphere template, and this shell could prevent the inside Ni surface from reacting with Sb^{3+} (step2). As a result, only the holes in the newly formed NiSb shells could serve as active sites for further reaction, allowing all the species involved in the reaction to continuously diffuse in and out of the holes until the Ni nanosphere template was completely digested[13] (step3). Besides providing electrons, Ni nanosphere template also served as support for Sb deposition and nucleation. During the process, Sb continued nucleating on the Ni nanosphere template surface, and which continued to be consumed until completely consumed. Finally, all holes were almost disappeared and each shell was characterized by a hole-free surface. The elimination of holes could be attributed to mass-transport processes like Ostwald ripening[14].

Therefore, the electrochemical performances of NiSb alloy HNSs as anode materials were investigated. Fig. 4a showed the typical cyclic voltammograms (CVs) of NiSb alloy HNSs electrode in the initial three cycles at a scan rate of 0.1 mV s^{-1} between 0.1 and 2 V. During the first cathodic sweep, the broad reduction peak from 0.8 to 0.1 V was ascribed to both the reduction of NiSb and the decomposition of the electrolyte to form solid electrolyte interphase (SEI) film, corresponding to capacity loss during the first cycle. However, from the second cycle onward, only a distinct peak at 0.5 V was found, which may be attributed to the formation of Li_3Sb alloy. In the anodic sweep, oxidation peaks at 1 V were assigned to the dealloying reaction of Li_3Sb. All peaks were reproducible and stabile after the first cycle, implying the reversibility of the electrochemical reactions of NiSb alloy HNSs electrode.

Fig. 4b displayed the voltage profiles of NiSb anode in first three cycles between 0.01 and 2.0 V at a current density of 100 mA g^{-1}. The voltage profiles were typical characteristics of a NiSb electrode[10]. The first discharge and charge capacities of NiS

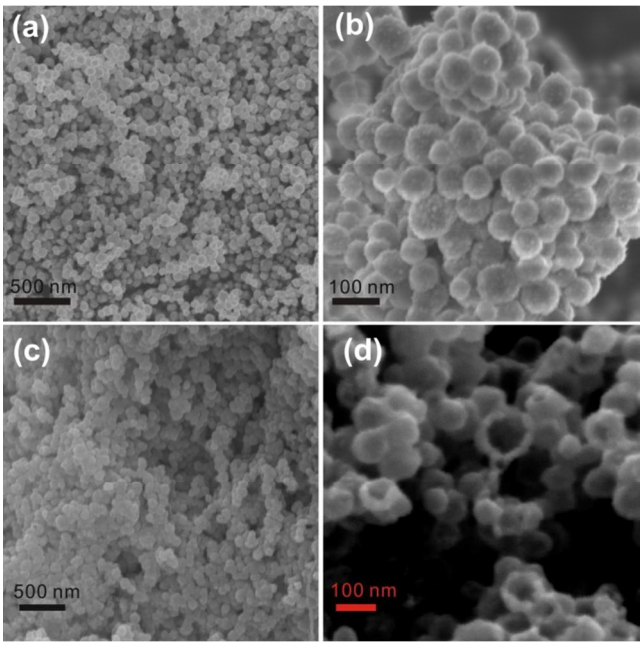

Fig. 1 SEM images of Ni nanopheres (a, b) and NiSb alloy HNSs (c, d).

NiSb were 577.2 and 444.8 mAh g^{-1} respectively, corresponding to a coulombic efficiency of 77.1%. The shape of the profiles did not change significantly during cycling, indicating the good stability of the NiSb alloy HNSs as an anode. This is in accordance with the CV curves (Fig. 4a). Because of the SEI layer formed on the anode, as well as the irreversible reaction, the the discharge capacity dropped from 577 to 445 mAh g^{-1} in the first two cycles.

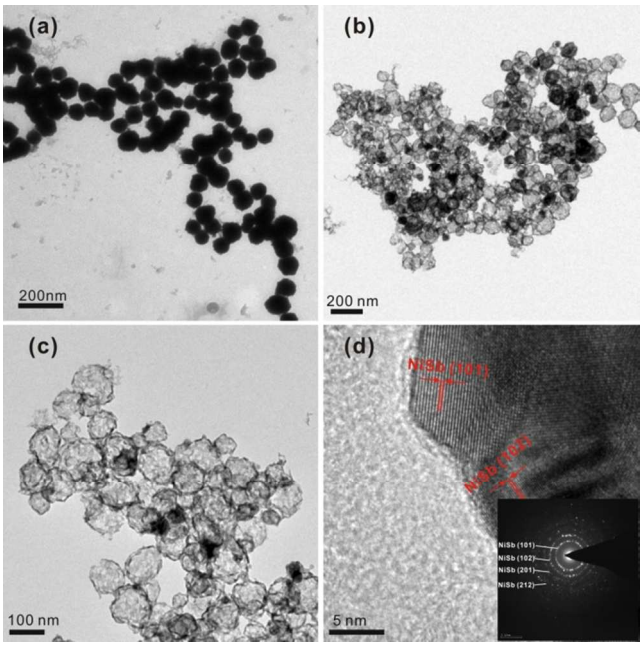

Fig. 2 TEM images of Ni nanopheres (a). TEM (b, c), HRTEM (d) images and SAED pattern (inset) of NiSb alloy HNSs.

Fig. 4c exhibited the cycle performance of as NiSb alloy HNSs at a current density of 100 mA g^{-1}. As can be seen, the NiSb alloy HNSs electrode showed superior cycle performance, delivering a high reversible capacity of 420 mAh g^{-1} after 50 cycles which is

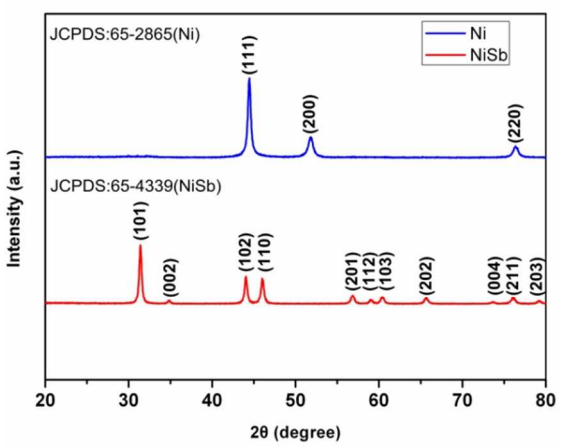

Fig. 3 XRD patterns of Ni NSs and NiSb alloy HNSs.

about 97.2 % of the reversible capacity (432 mAh g^{-1}) in the second cycle and it is in close proximity to the theoretical capacity (446 mAh g^{-1})[10] of NiSb alloy. The coulombic efficiency for the first cycle is around 77%, while it stabilized at ~98% for the following cycles. Unless stated, all the specific capacity values reported in this paper were calculated on the basis of the total mass of NiSb alloy.

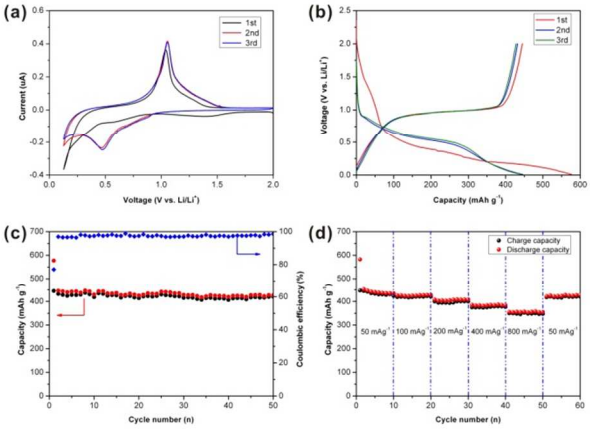

Fig. 4 Cycle performance (a), rate performance (b), galvanostatic charge-discharge profiles (c) and cyclic voltammograms (d) of NiSb alloy HNSs.

The rate performance of the HNSs was investigated at various currents ranging from 50 to 800 mA g^{-1}. As shown in Fig. 4d, when increasing the current density, NiSb exhibited decent reversible capacity retention: 433 mAh g^{-1} (50 mA g^{-1}), 420 mAh g^{-1} (100 mA g^{-1}), 401 mAh g^{-1} (200 mA g^{-1}), 377 mAh g^{-1} (400 mA g^{-1}), and 352 mAh g^{-1} (800 mA g^{-1}). At high current densities of 400 mA g^{-1} and 800 mA g^{-1}, the reversible capacities can also reach 377 mAh g^{-1} and 352 mAh g^{-1}. When the current density went back to 50 mA g^{-1}, the reversible capacity returned to 420 mAh g^{-1}, which was comparable to th e initial reversible capacity at 50 mA g^{-1}, indicating the electrode was stable and had high reversibility.

Note that the capacity of NiSb alloy HNSs is close to the theoretical capacity (446 mAh g^{-1}) after 50 cycles, it is much higher than that of other NiSb alloy based anode materials reported recently, such as NiSb-Al_2O_3-C nanocomposite[12], nanosized NiSb[15], NiSb nanocrystalline[16], NiSb/graphene[17]. It gives the best electrochemical performances for this type of alloy material (Table S1). The enhanced performances can be attributed to the unique structural characteristics of NiSb alloy HNSs. The Ni component serves as conductive and reinforcing matrix improved the conductivity and structure stability[9-12]. The thin shells greatly shorten the distances for Li^+ diffusion; the void space effectively accommodates the dramatic volume change and alleviates the strain during lithiation-delithiation[18].

In conclusion, NiSb alloy HNSs were prepared by galvanic replacement employing Ni NSs as templates. Compared with other NiSb alloy materials, the NiSb alloy HNSs showed higher capacity and significantly improved cycle performance. This type of hollow bimetalic nanospheres unique characteristics provides an attractive application in electrochemical energy storage devices and could be extended to the fabrication of various hollow bimetalic structures for a broad application in other fields, such as catalysis, photocatalysis, and gas sensing.

This work was financially supported by the National Natural Science Foundation of China (21003161 and 21250110060), the Program for the New Century Excellent Talents in University (NCET-11-0513) and the Distinguished Young Scientists of Hunan Province (13JJ1004).

Notes and references

*College of Chemistry and Chemical Engineering, Central South University, Changsha, China. Fax: +86-731-88879616; Tel: +86-731-88879616; E-mail: xji.csu.edu@gmail.com

† Electronic Supplementary Information (ESI) available: Details of preparation, characterization and electrochemical impedance spectroscopy (EIS) measurement. See DOI: 10.1039/b000000x/

1 W. Wei, Z. Wang, Z. Liu, Y. Liu, L. He, D. Chen, A. Umar, L. Guo and J. Li, *J. Power Sources*, 2013, **238**, 376-387.
2 X. Lai, J. E. Halpert and D. Wang, *Energy Environ. Sci.* 2012, **5**, 5604.
3 J. Chen, B. Wiley, J. McLellan, Y. Xiong, Z.-Y. Li and Y. Xia, *Nano lett.*, 2005, **5**, 2058-2062.
4 Q. Cui, Y. Sha, J. Chen and Z. Gu, J. *Nanopart. Res.*, 2011, **13**, 4785-4794.
5 X. Fan, X. Tang, D. Ma, P. Bi, A. Jiang, J. Zhu and X. Xu, *J. Solid State Electr.*, 2014, 1-9.
6 X. Lu, M. McKiernan, Z. Peng, E. P. Lee, H. Yang and Y. Xia, *Sci. Adv. Mater.*, 2010, **2**, 413-420.
7 M. Mohl, D. Dobo, A. Kukovecz, Z. Konya, K. Kordas, J. Wei, R. Vajtai and P. M. Ajayan, *J. Phys. Chem. C*, 2011, **115**, 9403-9409.
8 X. Xia, Y. Wang, A. Ruditskiy and Y. Xia, *Adv. Mater.*, 2013, **25**, 6313-6333.
9 J. Zhu, T. Sun, J. Chen, W. Shi, X. Zhang, X. Lou, S. Mhaisalkar, H. H. Hng, F. Boey and J. Ma, *Chem. Mater.*, 2010, **22**, 5333-5339.
10 E. Allcorn and A. Manthiram, *J. Phys. Chem. C*, 2014, **118**, 811-822.
11 E. Allcorn and A. Manthiram, *ACS Appl. Mater. Interfaces*, 2014, dx.doi.org/10.1021/am500448f.
12 Y. He, L. Huang, X. Li, Y. Xiao, G.L. Xu, J.T. Li and S.G. Sun, *J. Mater. Chem.*, 2011, **21**, 18517-18519.
13 Y. Sun, B. Mayers and Y. Xia, *Adv. Mater.*, 2003, **15**, 641-646.
14 Y. Sun and Y. Xia, *Nano lett.*, 2003, **3**, 1569-1572.
15 J. Xie, X. Zhao, H. Yu, H. Qi, G. Cao and J. Tu, *J. Alloys Compd.*, 2007, **441**, 231-235.
16 C. Li, J. Hu, Q. Peng and X. Wang, *Mater. Chem. and Phys.*, 2008, **110**, 106-109.
17 J. Xie, Y.X. Zheng, R.J. Pan, S.-Y. Liu, W.T. Song, G.S. Cao, T.J. Zhu and X.B. Zhao, *Int. J. Electrochem. Sci.*, 2011, **6**, 4811- 4821.
18 H. Kim and J. Cho, *Chem. Mater.*, 2008, **20**, 1679-1681.